AAS 19-801

SUN-AVOIDANCE SLEW PLANNING ALGORITHM WITH POINTING AND ACTUATOR CONSTRAINTS

Mohammad Ayoubi*and Junette Hsin†

This paper presents a geometric approach for a sun (or any bright object) avoidance slew maneuver with pointing and actuator constraints. We assume spacecraft has a single light-sensitive payload with control-torque and reaction wheels' angular momentum constraints. Furthermore, we assume the initial and final attitudes, instrument boresight vector, and sun vector are known. Then we use Pontryagin's minimum principle (PMP) and derive the desired or target-frame quaternions, angular velocity and acceleration. In the end, a Monte Carlo simulation is performed to show the viability of the proposed algorithm with control-torque and angular momentum constraints.

INTRODUCTION

Large-angle slew maneuvers are required during any Earth-pointing or interplanetary missions. In many space missions, and for safety consideration, a sensitive payload such as imaging camera or telescope needs to be retargeted while avoiding the sun vector or other bright objects in the sky. The attitude reorientation problem in the presence of attitude constrained zones has been studied in the last three decades. McInnes[1] addressed this problem via an artificial potential function. He proposed an entirely analytical guidance law which was suitable for onboard implementation. However, he used Euler angles, which are singular for large slew angles. A geometric approach was proposed by Spindle,[2] Hablani,[3] and Biggs and Colley[4] where a feasible attitude maneuver, or a guidance law, is precomputed based on the attitude-avoidance-zone constraints. Another approach for addressing this problem used randomized algorithms.[5] However, depending on the number of constraints and initial and final attitudes, this approach can be computationally expensive and not suitable for onboard implementation. Another approach for solving the time optimal reorientation maneuver subject to boundaries and path constraints was proposed by Spiller et al.[6] They used the particle swarm optimization (PSO) technique to find a sub-optimal solution with keep-out constraints. Another approach casted the problem as a convex optimization problem and used semi-definite programming (SDP) or quadratically constrained quadratic programming (QCQP) in its solution (see for instance Kim and Mesbahi,[7] Kim

*Associate Professor, Department of Mechanical Engineering, Santa Clara University, 500 El Camino Real, Santa Clara, CA 95053 U.S.A. AIAA senior member, AAS senior member.

†Engineer, Dynamics and Control Analysis Group, Maxar Space Infrastructure (formerly Space Systems/Loral), 3825 Fabian Way, Palo Alto, CA 94303 U.S.A.

et al.,[8] Sun and Dai,[9] and Lee and Mesbahi[10]). Recently, Ramos and Schaub[11] proposed a method based on the Lyapunov stability theorem and logarithmic barrier potential function to derive a steering law for attitude control of a spacecraft subject to conically constrained inclusion and exclusion regions. They also considered the control-torque constraint in their algorithm.

In this paper, we present a novel geometric approach for large-angle slew planning with pointing and actuator constraints. We assume that the spacecraft has a single light-sensitive payload with control-torque and reaction wheels' angular momentum constraints. Furthermore, we assume that the initial and final attitudes, instrument boresight vector, and sun vector are known. Then, we derive the desired or target-frame quaternions, angular velocities, and angular accelerations based on the Pontryagin's minimum principle (PMP) for the proposed maneuver. The proposed algorithm in this paper is intuitive, deterministic, easy to implement, and includes the control-torque and reaction wheels' angular momentum constraints. The main drawback of the proposed algorithm is its limitation for a single sensitive-payload. A Monte Carlo simulation is performed to show the viability of the proposed algorithm with control-torque and angular momentum constraints.

PROBLEM FORMULATION

Consider a gyrostat, (a rigid body with reaction wheels) and let us define a newtonian frame, N, and a gyrostat-centered unit sphere frame G with a center G^* as shown in Fig. 1. The sun or bright-object avoidance planning problem can be stated as follows:

Assume the initial state, $x_i = \left[{}_{\mathcal{N}}\hat{P}_i, {}^{\mathcal{N}}_{\mathcal{G}}\omega^{\mathcal{G}}(t_i), {}^{\mathcal{N}}q^{\mathcal{G}}(t_i)\right] \in \mathbb{R}^3 \times \mathbb{R}^3 \times \mathbb{SO}(3)$, final state, $x_f = \left[{}_{\mathcal{N}}\hat{P}_f, {}^{\mathcal{N}}_{\mathcal{G}}\omega^{\mathcal{G}}(t_f), {}^{\mathcal{N}}q^{\mathcal{G}}(t_f)\right] \in \mathbb{R}^3 \times \mathbb{R}^3 \times \mathbb{SO}(3)$, the sun unit vector in the inertial frame, ${}_{\mathcal{N}}\hat{S} \in \mathbb{R}^3$, the sensitive instrument boresight unit vector in the body-fixed frame, ${}_{\mathcal{G}}\hat{P} \in \mathbb{R}^3$, and the half-cone angle $\epsilon_p \in \mathbb{R}$ are given.

Find: A sequence of slew maneuvers such that the sun vector does not enter into the on-board sensitive instrument forbidden cone for all times $t \in [t_i, t_f]$ subject to actuator constraints.

SUN-AVOIDANCE SLEW (SAS) ALGORITHM DESCRIPTION

The first step is to determine if there is the sun vector intrusion. To this end, we check the angular separation, α, between the sun unit vector, ${}_{\mathcal{N}}\hat{S}$, and the $\hat{P}_i - \hat{P}_f$ plane, or "slew plane,"

$$\alpha = \frac{\pi}{2} - \cos^{-1}(\hat{S} \cdot \hat{e}) \tag{1}$$

where the eigenaxis unit vector is determined by

$$\hat{e} = \frac{\hat{P}_i \times \hat{P}_f}{|\hat{P}_i \times \hat{P}_f|}. \tag{2}$$

If $|\alpha| >= \epsilon_p$ then the sun vector intrusion has not happened. Otherwise, we need to perform sun-avoidance slew maneuver which is explained in the next section.

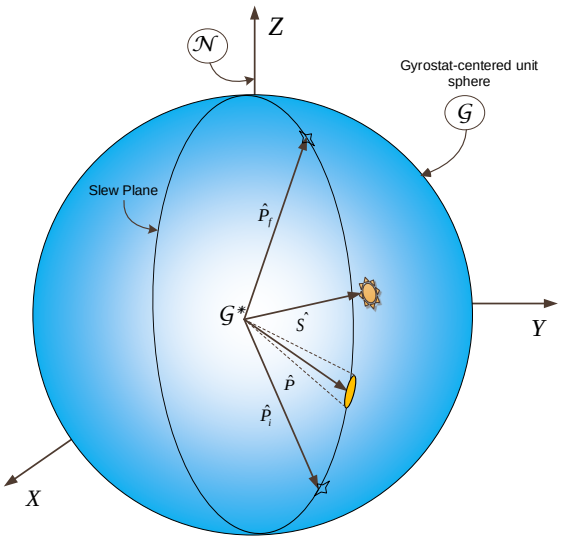

Figure 1. Gyrostat-centered unit sphere centered at point $\mathcal{G}^*$.

Slew Planning If $|\alpha| < \epsilon_p$, then we need to plan the sun-avoidance slew in the following steps:

1. The 1^{st} slew is around the eigenaxis, $\hat{e}$, through angle ϕ_1:

$$\phi_1 = \cos^{-1}(\hat{P}_i \cdot_{\mathcal{G}} \hat{S}_{||}) - \epsilon_p \tag{3}$$

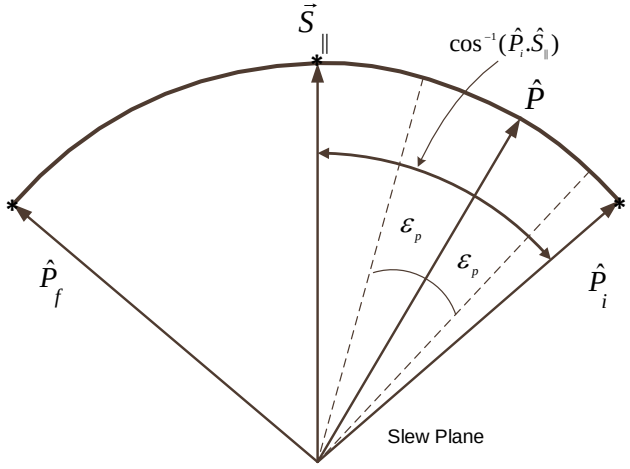

Figure 2. View of the sensitive instrument boresight vector motion during the 1^{st} slew from above the slew plane.

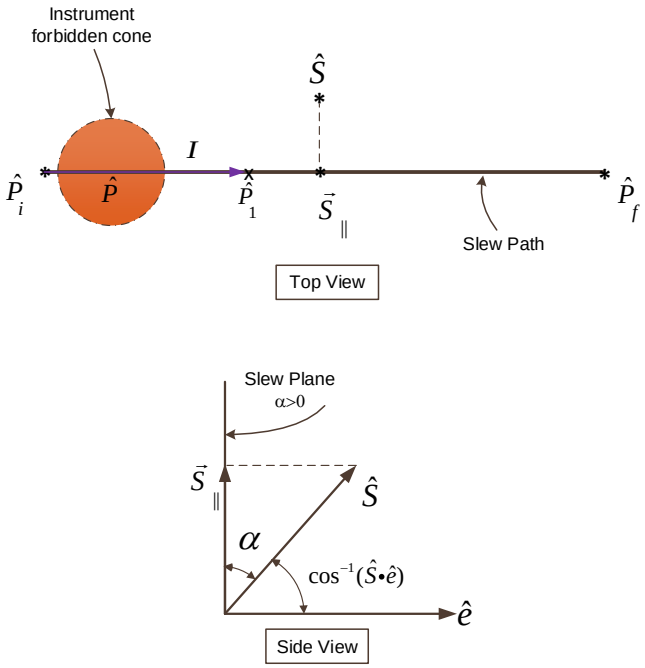

Figure 3. Top and side views of the sensitive instrument boresight vector motion during the 1^{st} slew.

where

$$\vec{S}_{||} = \hat{S}\cos\alpha, \tag{4}$$

and

$$\hat{S}_{||} = \frac{\vec{S}}{|\vec{S}|}. \tag{5}$$

It should be noted that the vector $\hat{S}_{||}$ is in the $\mathcal{N}$-frame. Therefore, it should be transformed in the $\mathcal{G}$-frame before it can be used in Eq. (3).

2. The 2^{nd} slew is around the unit sun vector, $\hat{S}$, via angle ϕ_2.

   (a) when $\alpha \neq 0$

$$\phi_2 = 2\tan^{-1}\left[\frac{\hat{S}\cdot(\hat{P}_1\times\hat{S}_{||})}{(\hat{P}_1\cdot\hat{S}_{||}) - (\hat{S}\cdot\hat{P}_1)(\hat{S}\cdot\hat{S}_{||})}\right], \tag{6}$$

   or

$$\phi_2 = 2\tan^{-1}\left[\frac{(\pi/2-\alpha)\sin\epsilon_p}{\cos\epsilon_p - \cos\theta\cos\alpha}\right] \tag{7}$$

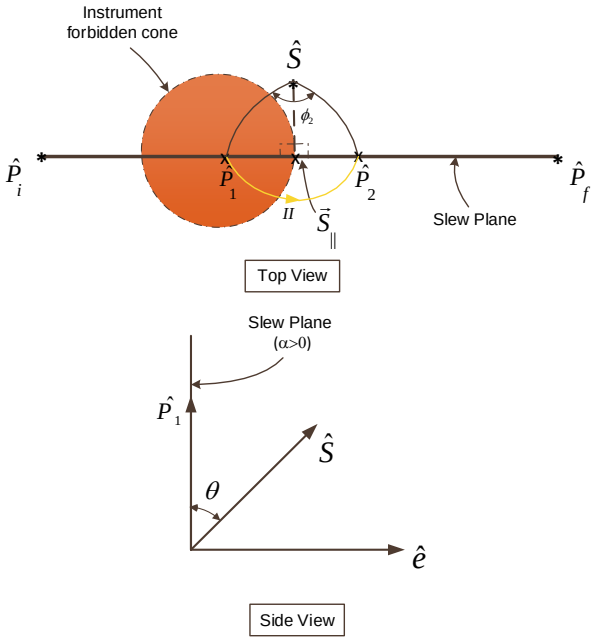

Figure 4. The sensitive instrument boresight vector motion during the 2^{nd} slew when $\alpha \neq 0$.

(b) when $\alpha = 0$

$$\phi_2 = \pi \tag{8}$$

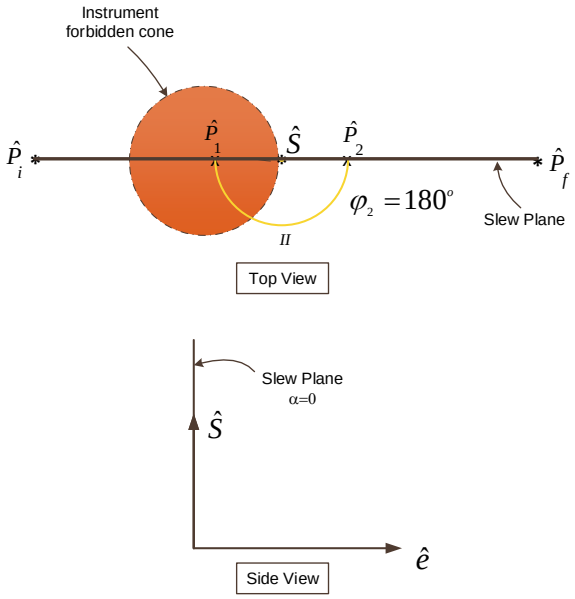

Figure 5. The sensitive instrument boresight vector motion during the 2^{nd} slew when $\alpha = 0$.

3. The 3^{rd} slew is about the $\hat{e}$ through angle ϕ_3:

$$\phi_3 = \cos^{-1}({}_{\mathcal{G}}\hat{P}_f \cdot \hat{P}_2) \tag{9}$$

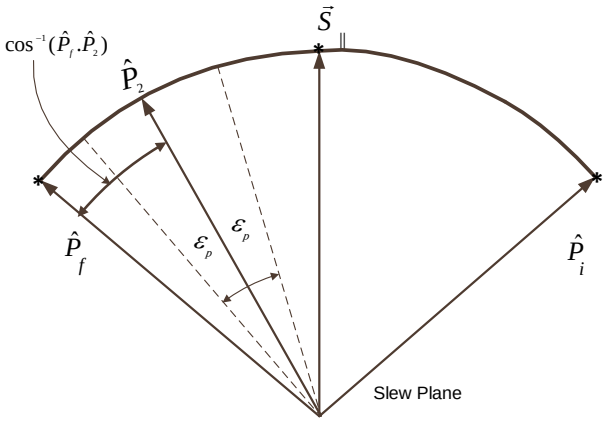

Figure 6. The sensitive instrument boresight vector motion during the 3^{rd} slew.

Similar to the 1^{st} maneuver, the vector ${}_{\mathcal{N}}\hat{P}_f$ needs to be transformed to the $\mathcal{G}$-frame before doing the dot product in Eq. (9).

4. The final slew about the instrument boresight axis may be needed to go to the final attitude.

Summary of Algorithm

1. Slew around the eigenaxis, $\hat{e}$, through angle ϕ_1:

$$\phi_1 = \cos^{-1}(\hat{P}_i \cdot_{\mathcal{G}} \hat{S}_{||}) - \epsilon_p \tag{10}$$

2. Slew around the $\hat{S}$ via:

$$\phi_2 = \begin{cases} 2\tan^{-1}\left[\frac{(\pi/2-\alpha)\sin\epsilon_p}{\cos\epsilon_p - \cos\theta\cos\alpha}\right] & when\ \alpha \neq 0 \\ \pi & when\ \alpha = 0 \end{cases} \tag{11}$$

3. Slew about the $\hat{e}$ through angle:

$$\phi_3 = \cos^{-1}({}_{\mathcal{G}}\hat{P}_f \cdot \hat{P}_2) \tag{12}$$

4. If necessary, perform the final rotation, ϕ_4, about the instrument boresight axis to adjust the attitude.

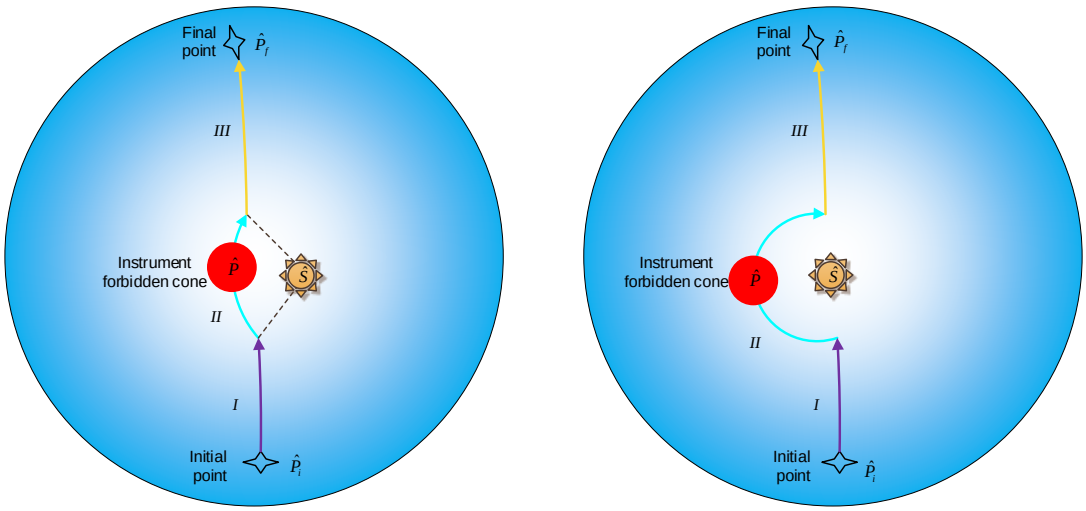

Figure 7. The trajectory of the instrument boresight tip on the gyrostat-centered unit sphere during the SAS maneuver.

STEERING LAWS

In this section we utilize the proposed sun-avoidance slew algorithm to generate the required angular rate, ${}^{\mathcal{N}}_{\mathcal{G}}\omega^{\mathcal{T}}$, angular acceleration, ${}^{\mathcal{N}}_{\mathcal{G}}\alpha^{\mathcal{T}}$, and quaternions, ${}^{\mathcal{N}}q^{\mathcal{T}}$, for the control system. Fig. 8 shows how the generated commands are utilized by an attitude control system to guide the gyrostat in each leg of the SAS.

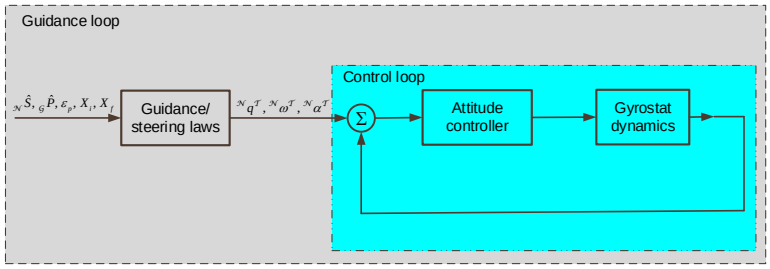

Figure 8. Block diagram of guidance and control loops.

In the following, we formulate the problem of finding the steering laws for two cases with: 1) velocity and acceleration constraints and 2) acceleration constraint.

Case 1: Single-Axis, Agile Slew Maneuver with Velocity and Acceleration Constraints.

Problem Statement: Consider the motion of a gyrostat around a given inertially-fixed axis, ${}_{\mathcal{N}}\hat{e}$, as shown in Fig. 9. The problem of minimum-time slew maneuver around the ${}_{\mathcal{N}}\hat{e}$-axis can be formulated as:

$$\underset{u\in\mathcal{U}}{Minimize}\ \mathcal{J}[x(.),u(.),t_f] = \int_{t0}^{t_f} dt, \tag{13}$$

subject to the following dynamic constraints:

$$\Sigma_{\mathcal{G}} : \begin{cases} \dot{x}_1 = x_2, \\ \dot{x}_2 = M/I_{\hat{e}}^{\mathcal{G}/\mathcal{G}*} = u, \end{cases} \tag{14}$$

where $\mathcal{U}$ is a set of all admissible controls, $x_1 \triangleq \phi$, $x_2 = \dot{\phi}$, and M is the projection of the reaction wheel or other actuators torque along the $\hat{e}$, and

$$I_{\hat{e}}^{\mathcal{G}/\mathcal{G}*} = \hat{e}\, I^{\mathcal{G}/\mathcal{G}*}\, \hat{e}^T. \tag{15}$$

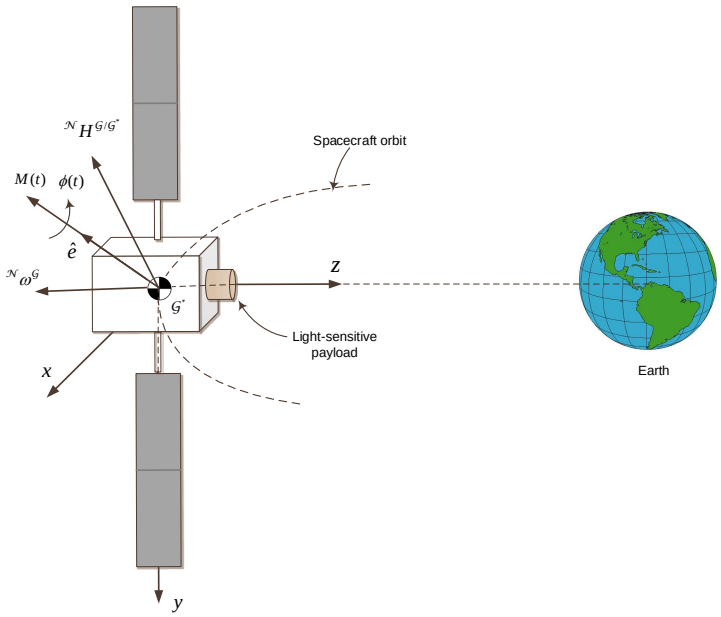

Figure 9. A gyrostat rotating about the eigenaxis, $\hat{e}$,

where T denotes transpose. The boundary conditions are given by

$$BCs : \begin{cases} \phi(t_0) = 0, \phi(t_f) = \phi_f, \\ \dot{\phi}(t_0) = \dot{\phi}_0, \dot{\phi}(t_f) = \dot{\phi}_f, \end{cases} \tag{16}$$

and the reaction wheels' angular momentum and control-torque acceleration can be transformed into the angular velocity and angular acceleration constraints as follows

$$C_1 : \begin{cases} |x_2 = \dot{\phi}| \leq \dot{\phi}_{max}, \\ |u = \ddot{\phi}| \leq \ddot{\phi}_{max}, \end{cases} \tag{17}$$

where ${}^{\mathcal{N}}H^{\mathcal{G}/\mathcal{G}*}$ is the total angular momentum of the gyrostat with respect to its center of mass, $\mathcal{G}^*$, in the $\mathcal{N}$-frame. $I^{\mathcal{G}/\mathcal{G}^*}$ and $I^{w/w*}$ represent the mass-moment-of-inertia of the gyrostat and reaction wheels with respect to their center of masses, respectively. M_{max} is the maximum available torque along the eigenaxis in the $\mathcal{G}$-frame. Our objective is to find ${}^{\mathcal{N}}\omega^{\mathcal{T}}(t)$, ${}^{\mathcal{N}}\alpha^{\mathcal{T}}(t)$, and ${}^{\mathcal{N}}q^{\mathcal{T}}(t)$.

Using the optimal control theory and Pontryagin's minimum principle (PMP), we derive the necessary conditions for the optimal solution as follows:

1. State Eqs.:

$$\begin{cases} \dot{x}_1 = x_2, \\ \dot{x}_2 = u, \\ \dot{x}_3 = (x_2 + \dot{\phi}_{max})^2 \mathbb{U}(-x_2 - \dot{\phi}_{max}) + (\dot{\phi}_{max} - x_2)^2 \mathbb{U}(x_2 - \dot{\phi}_{max}), \end{cases} \tag{18}$$

   where the unit step function, $\mathbb{U}$, is defined as

$$\mathbb{U}(X) = \begin{cases} 1, X > 0, \\ 0, X \leq 0. \end{cases} \tag{19}$$

   Note: $(x_3(t_0) = x_3(t_f) = 0$ & $x_3(t) \geq 0\ ) \rightarrow x_3(t) = 0, t \in [t_0, t_f]$.

2. Hamiltonian:

$$\begin{aligned} \mathscr{H} =& 1 + \lambda_1 x_2 + \lambda_2 u + \lambda_3 \Big[(x_2 + \dot{\phi}_{max})^2 \mathbb{U}(-x_2 - \dot{\phi}_{max}) \\ & (\dot{\phi}_{max} - x_2)^2 \mathbb{U}(x_2 - \dot{\phi}_{max}) \Big] \end{aligned} \tag{20}$$

3. Costate Eqs.:

$$\begin{cases} \dot{\lambda}_1 = -\frac{\partial \mathscr{H}}{\partial x_1} = 0, \\ \dot{\lambda}_2 = -\frac{\partial \mathscr{H}}{\partial x_2} = -\lambda_1 - 2\lambda_3 (x_2 + \dot{\phi}_{max}) \mathbb{U}(-x_2 - \dot{\phi}_{max}) \\ +2\lambda_3 (\dot{\phi}_{max} - x_2) \mathbb{U}(x_2 - \dot{\phi}_{max}), \\ \dot{\lambda}_3 = -\frac{\partial \mathscr{H}}{\partial x_3} = 0. \end{cases} \tag{21}$$

4. Applying the Pontryagin's minimum principle (PMP),

$$u^* = \underset{u \in \mathcal{U}}{argmin} \mathscr{H}, \tag{22}$$

where $\mathcal{U}$ defines the domain of feasible controls. The optimal control can be determined as

$$u^*(t) = \begin{cases} \ddot{\phi}_{max} & \lambda_2 < 0, \\ ? & \lambda_2 = 0, \\ -\ddot{\phi}_{max} & \lambda_2 > 0. \end{cases} \tag{23}$$

This is a *singular arc* optimal control problem.

5. Determining the optimal control in the singular arc:

$$\frac{d^2}{dt^2}\Big(\frac{\partial \mathscr{H}}{\partial u}\Big) = \ddot{\lambda}_2 = 0 \rightarrow \dot{x}_2 = 0 \rightarrow u^* = 0 \tag{24}$$

6. Checking the Generalized Legendre-Clebsch condition for optimality:

$$(-1)^2 \frac{\partial}{\partial u}\Big[\frac{d^2}{dt^2}\Big(\frac{\partial \mathscr{H}}{\partial u}\Big)\Big] = 1 \geq 0 \tag{25}$$

7. Checking the transversality condition:

$$\mathscr{H}|_{(*,t_f)} = 0 \text{ and } \mathscr{H} \neq \mathscr{H}(t) \rightarrow \mathscr{H} = 0, \forall t \in [t_0, t_f]. \tag{26}$$

The angular acceleration profile is bang-off-bang, as shown in Fig. 10

$$\ddot{\phi}(t) = u = \begin{cases} \ddot{\phi}_{max} & when\ t_0 \leq t \leq t_1, \\ 0 & when\ t_1 \leq t \leq t_2, \\ -\ddot{\phi}_{max} & when\ t_2 \leq t \leq t_f. \end{cases} \tag{27}$$

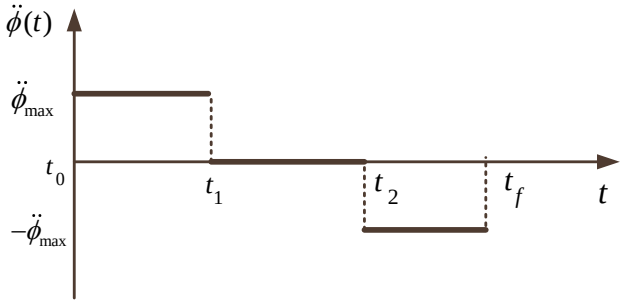

Figure 10. The optimal control law for case 1.

The angular velocity profile can be determined as

$$\dot{\phi}(t) = \begin{cases} \dot{\phi}_0 + \ddot{\phi}_{max}(t - t_0) & when\ t_0 \leq t \leq t_1, \\ \dot{\phi}_{max} & when\ t_1 \leq t \leq t_2, \\ \dot{\phi}_{max} - \ddot{\phi}_{max}(t - t_2) & when\ t_2 \leq t \leq t_f. \end{cases} \tag{28}$$

and the angular position can be find by direct integration of Eq. (28),

$$\phi(t) = \begin{cases} \dot{\phi}_0(t-t_0) + \frac{1}{2}\ddot{\phi}_{max}(t-t_0)^2 & when\ t_0 \leq t \leq t_1, \\ \phi(t_1) + \dot{\phi}_{max}(t-t_1) & when\ t_1 \leq t \leq t_2, \\ \phi(t_2) + \dot{\phi}_{max}(t-t_2) - \frac{1}{2}\ddot{\phi}_{max}(t-t_2)^2 & when\ t_2 \leq t \leq t_f. \end{cases} \tag{29}$$

Using the conditions, $\dot{\phi}(t_1) = \dot{\phi}_{max}$, $\dot{\phi}(t_f) = \dot{\phi}_f$, $\phi(t_f) = \phi_f$, we can determine switching times t_1, t_2, and final time t_f. Depending on the size of ϕ and the maximum velocity and acceleration constraints, the spacecraft may or may not reach its maximum allowed velocity during a slew, which in turn determines the calculation of switching times. There is a threshold angle, which is called ϕ_t and is calculated from the constraints:

$$\phi_t = \frac{\dot{\phi}_{max}^2}{\ddot{\phi}_{max}}. \tag{30}$$

If $\phi > \phi_t$, then there will be period of coasting at constant velocity (at the maximum velocity constraint) in between the periods of acceleration and deceleration during the slew. In such a case, we can determine switching times t_1, t_2, and final time t_f as

$$t_1 = t_0 + \frac{\dot{\phi}_{max} - \dot{\phi}_0}{\ddot{\phi}_{max}}, \tag{31}$$

$$\begin{aligned} t_2 =& t_1 + \frac{1}{\dot{\phi}_{max}}\Big[\phi_f - \dot{\phi}_0(t_1 - t_0) - \frac{1}{2}\ddot{\phi}_{max}(t_1 - t_0)^2 \\ & - \frac{\dot{\phi}_{max}(\dot{\phi}_{max} - \dot{\phi}_f)}{\ddot{\phi}_{max}} + \frac{(\dot{\phi}_{max} - \dot{\phi}_f)^2}{2\ddot{\phi}_{max}}\Big], \end{aligned} \tag{32}$$

and

$$t_f = t_1 + \frac{1}{\dot{\phi}_{max}}\Big[\phi_f - \dot{\phi}_0(t_1 - t_0) - \frac{1}{2}\ddot{\phi}_{max}(t_1 - t_0)^2 + \frac{(\dot{\phi}_{max} - \dot{\phi}_f)^2}{2\ddot{\phi}_{max}}\Big]. \tag{33}$$

Otherwise, if $\phi \leq \phi_t$, then there will be no period of coasting at angular velocity, and the acceleration profile of the spacecraft will be changing from the initial to the final point of the slew. The switching times are then are determined by:

$$t_f = \sqrt{\frac{4\phi}{\ddot{\phi}_{max}}} \tag{34}$$

$$t_2 = \frac{t_f}{2} \tag{35}$$

$$t_1 = t_2 \tag{36}$$

The target steering profiles including the quaternions, angular rate, and angular acceleration can be determined as

$$^{\mathcal{N}}q^{\mathcal{T}}(t) = \Big[e_x \sin\frac{\phi(t)}{2}, e_y \sin\frac{\phi(t)}{2}, e_z \sin\frac{\phi(t)}{2}, \cos\frac{\phi(t)}{2}\Big]^T, \tag{37}$$

$$^{\mathcal{N}}\omega^{\mathcal{T}}(t) = \dot{\phi}(t)\, ^{\mathcal{G}}R^{\mathcal{N}}\, _{\mathcal{N}}\hat{e}, \tag{38}$$

$$^{\mathcal{N}}\alpha^{\mathcal{T}}(t) = \ddot{\phi}(t)\, ^{\mathcal{G}}R^{\mathcal{N}}\, _{\mathcal{N}}\hat{e}, \tag{39}$$

where the transformation matrix from the $\mathcal{N}$-frame to $\mathcal{G}$-frame, $^{\mathcal{G}}R^{\mathcal{N}}$ is given by

$$^{\mathcal{G}}R^{\mathcal{N}} = \big[(cos\phi)\mathbb{I}_{3x3} + (1 - cos\phi)\hat{e}\hat{e}^T - (sin\phi)\hat{e}^{\times}\big], \tag{40}$$

and the skew-symmetric matrix $\hat{e}^{\times}$ is defined in terms of components of the $\hat{e}$ as

$$\hat{e}^{\times} = \begin{bmatrix} 0 & -e_3 & e_2 \\ e_3 & 0 & -e_1 \\ -e_2 & e_1 & 0 \end{bmatrix}. \tag{41}$$

It is worth mentioning here that the computed $^{\mathcal{N}}\omega^{\mathcal{T}}(t)$ and $^{\mathcal{N}}\omega^{\mathcal{T}}(t)$ given by Eqs. (38)–(39) are expressed in the $\mathcal{G}$-frame. The required body-torque, $u \in \mathcal{R}^{3\times 1}$, can be determined from the Euler's dynamical law as

$$u = J^{\mathcal{G}/\mathcal{G}^*}\, ^{\mathcal{N}}\alpha^{\mathcal{T}} + ^{\mathcal{N}}\omega^{\mathcal{T}} \times J^{\mathcal{G}/\mathcal{G}^*}\, ^{\mathcal{N}}\omega^{\mathcal{T}}. \tag{42}$$

And finally, the attitude and angular velocity of the gyrostat can be found from the kinematical equation of motion:

$$\dot{q} = \frac{1}{2}\Omega q, \tag{43}$$

where Ω is

$$\Omega = \begin{bmatrix} 0 & \omega_3 & -\omega_2 & \omega_1 \\ -\omega_3 & 0 & -\omega_1 & \omega_2 \\ \omega_2 & -\omega_1 & 0 & \omega_3 \\ -\omega_1 & \omega_2 & -\omega_3 & 0 \end{bmatrix} \tag{44}$$

Equations (27)–(44) can be used with proper boundary conditions to determine the steering laws for each segment of the SAS algorithm. This is shown in the next section for the acceleration constraint case.

Case 2: Single-Axis, Agile Slew Maneuver with Acceleration Constraint

Problem Statement: Consider the optimal control problem described by Eqs. (13), (14)–(16), subject to control constraint

$$C_2 : \ |u = \ddot{\phi}| \leq \ddot{\phi}_{max}, \tag{45}$$

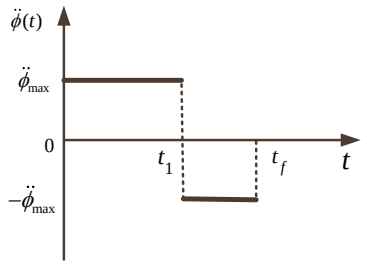

Figure 11. The optimal control in case 2.

and find ${}^{\mathcal{N}}\omega^{\mathcal{T}}(t)$, ${}^{\mathcal{N}}\alpha^{\mathcal{T}}(t)$, and ${}^{\mathcal{N}}q^{\mathcal{T}}(t)$ for the SAS maneuver.

It is well known that the angular acceleration about the $\hat{e}$ axis is a bang-bang control as shown in Fig. 11.

$$\ddot{\phi}(t) = \ddot{\phi}_{max}\mathbb{U}(t_0) - 2\ddot{\phi}_{max}\mathbb{U}(t - t_1), \tag{46}$$

where the switching and the final times are given by

$$t_1 = t_0 - \frac{\dot{\phi}_0}{\ddot{\phi}_{max}} + \frac{\sqrt{\ddot{\phi}^2_{max}(2\ddot{\phi}_{max}\phi_f + \dot{\phi}^2_f + \dot{\phi}^2_0)}}{\sqrt{2}\ddot{\phi}^2_{max}}, \tag{47}$$

and

$$t_f = t_0 - \frac{\dot{\phi}_f + \dot{\phi}_0}{\ddot{\phi}_{max}} + \frac{\sqrt{2}\sqrt{\ddot{\phi}^2_{max}(2\ddot{\phi}_{max}\phi_f + \dot{\phi}^2_{ef} + \dot{\phi}^2_0)}}{\ddot{\phi}^2_{max}}. \tag{48}$$

The angular velocity and angular rate about the $\hat{e}$ axis are

$$\dot{\phi}(t) = \dot{\phi}_0 + \ddot{\phi}_{max}(t - t_0)\mathbb{U}(t_0) - 2\ddot{\phi}_{max}(t - t_1)\mathbb{U}(t - t_1), \tag{49}$$

$$\phi(t) = \dot{\phi}_0(t - t_0) + \ddot{\phi}_{max}\frac{(t - t_0)^2}{2}\mathbb{U}(t_0) - 2\ddot{\phi}_{max}\frac{(t - t_1)^2}{2}\mathbb{U}(t - t_1). \tag{50}$$

The First Slew Maneuver: This is a single-axis nonrest-to-rest maneuver around the $\hat{e}$ with boundary conditions,

$$\dot{\phi}(t_0) = \dot{\phi}_0, \phi(t_0) = 0, \dot{\phi}(t_{f1}) = 0, \phi(t_{f1}) = \phi_1. \tag{51}$$

The switching time, t_{11}, and the minimum-time, t_{f1}, are

$$t_{11} = t_0 - \frac{\dot{\phi}_0}{\ddot{\phi}_{max}} + \frac{\sqrt{\ddot{\phi}^2_{max}(2\ddot{\phi}_{max}\phi_1 + \dot{\phi}^2_0)}}{\sqrt{2}\ddot{\phi}^2_{max}}, \tag{52}$$

$$t_{f1} = t_0 - \frac{\dot{\phi}_0}{\ddot{\phi}_{max}} + \frac{\sqrt{2\ddot{\phi}^2_{max}(2\ddot{\phi}_{max}\phi_1 + \dot{\phi}^2_0)}}{\ddot{\phi}^2_{max}}. \tag{53}$$

The Second Slew Maneuver: This is a rest-to-rest maneuver around the sun vector with boundary conditions given by

$$\dot{\phi}(t_0) = 0, \phi(t_0) = 0, \dot{\phi}(t_{f2}) = 0, \phi(t_{f2}) = \phi_2. \tag{54}$$

The switching time, t_{12}, and the minimum-time, t_{f2}, are

$$t_{12} = t_0 - \frac{\sqrt{\phi_2}}{\ddot{\phi}_{max}}, \tag{55}$$

$$t_{f2} = t_0 - \frac{2\sqrt{\phi_2}}{\ddot{\phi}_{max}}. \tag{56}$$

The Third Slew Maneuver: This is a single-axis rest-to-nonrest maneuver around the $\hat{e}$ with boundary conditions,

$$\dot{\phi}(t_0) = 0, \phi(t_0) = 0, \dot{\phi}(t_{f3}) = \dot{\phi}_f, \phi(t_{f3}) = \phi_3. \tag{57}$$

The switching time, t_{13}, and the minimum-time, t_{f3}, are

$$t_{13} = t_0 + \frac{\sqrt{\ddot{\phi}^2_{max}(2\ddot{\phi}_{max}\phi_3 + \dot{\phi}^2_f)}}{\sqrt{2}\ddot{\phi}^2_{max}}, \tag{58}$$

$$t_{f3} = t_0 - \frac{\dot{\phi}_f}{\ddot{\phi}_{max}} + \frac{\sqrt{2\ddot{\phi}^2_{max}(2\ddot{\phi}_{max}\phi_3 + \dot{\phi}^2_f)}}{\ddot{\phi}^2_{max}}. \tag{59}$$

Knowing the switching time for each slew, the $\ddot{\phi}(t)$, $\dot{\phi}(t)$, and $\phi(t)$, can be found by substituting the boundary conditions for each slew in to Eqs. (46), (49), and (50), respectively. Then the steering laws, i.e. ${}^{\mathcal{N}}\omega^{\mathcal{T}}(t)$, ${}^{\mathcal{N}}\alpha^{\mathcal{T}}(t)$, ${}^{\mathcal{N}}q^{\mathcal{T}}(t)$, can be found from Eqs. (37)–(44).

NUMERICAL SIMULATION

We used MATLAB® to examine and validate the proposed algorithm in this paper. The initial, final, and sun position vectors were selected randomly such that the initial and final positions end up outside of the exclusion zone. The progression of the spacecraft along its orbit was not incorporated in these simulations, therefore, the sun vector does not change during the slew maneuvers. However, when the orbit is taken into account during real missions, the location of the sun vector during the ϕ_2 portion of the maneuvers should be considered. Or rather, the timing of the instrument boresight overlapping with the sun vector projection onto the slew plane should be used in the calculation of the slew angles. The pseudocode for the proposed SAS algorithm is shown Algorithm 1.

In the following, we present the results of two cases: I) when the sun angle does not lie in the slew plane, $|\alpha| > 0$, and II) when the sun vector lies in the slew plane, $\alpha = 0$. The parameters used in both cases are listed in Table 1. In case I, when $|\alpha| > 0$, the spacecraft slews from the initial to the target position during the maneuvers, and P_1 and P_2

Algorithm 1 A Pseudocode for the SAS Algorithm

Find eigenaxis, ${}_{\mathcal{N}}e$ of slew plane
    Compute cross product of P_i and P_f unit vectors
Compute angle between sun vector and slew plane angle α
if $|\alpha| < \epsilon_p$ **then**
    Execute sun-avoidance slew:
        Find $\vec{S}_{||}$
        Compute ϕ_1, ϕ_2, ϕ_3
    Compute ϕ_t
    Compute switching times t_1, t_2, t_f for ϕ_1, ϕ_2, and ϕ_3:
    if $\phi > \phi_t$ **then**
        Use equations 31 through 33
    else
        Use equations 34 through 36
    end if
    for $t_0 < t < t_1$ **do**
        Calculate inertial-to-desired rotation ${}^{\mathcal{T}}R^{\mathcal{N}}$
        From ${}^{\mathcal{T}}R^{\mathcal{N}}$, calculate ${}_{\mathcal{G}}\dot{\omega}^{\mathcal{T}}$
            Solve for control torque u with equation 42
            Propagate ω and q by solving equations 42 and 43
    end for
    Repeat above lines for $t_1 < t < t_2$ and $t_2 < t < t_f$
else
    Slew directly from P_i to P_f
end if

Table 1. Initial, Final, and Sun Positions in Inertial Frame and Constraints Used in the Simulation

Case	Symbol	Unit Vector	$\dot{\phi}_{max}$	$\ddot{\phi}_{max}$
I)	$\hat{P}_i$	$[-0.50, 0.57, 0.65]$	$1\ (rad/s)$	$1\ (rad/s^2)$
	$\hat{P}_f$	$[0.76, -0.48, -0.44]$		
	$\hat{S}$	$[0.30, -0.50, -0.81]$		
II)	P_i	[0.65, -0.35, -0.67]	$0.01\ (rad/s)$	$0.02\ (rad/s^2)$
	P_f	[-0.93, -0.25, 0.28]		
	S	[-0.20, -0.78, -0.59]		

are connected via a rotation around the sun vector as shown in Fig. 12. The computed slew angles in this case are $(32.08, 102.56, 17.76)^\circ$.

The time histories of angular velocity and angular acceleration are shown in Fig. 15. In real missions, the spacecraft's reaction wheels' ability to impart angular momentum is translated to a constraint in angular velocity, and the thrusters ability to impose torque

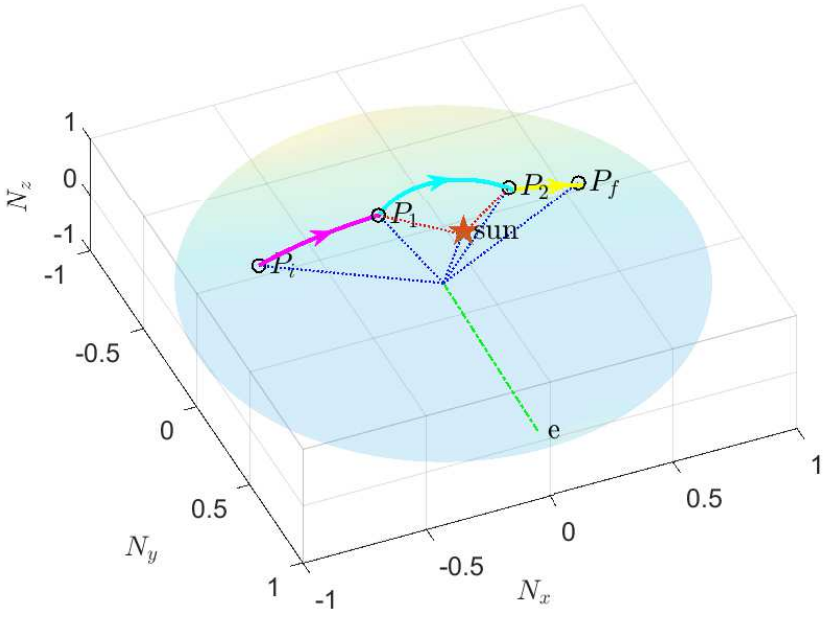

Figure 12. boresight during the entire slew when $|\alpha| > 0$.

translates to a constraint in angular acceleration. Therefore, no torque constraint is considered in this simulation. Due to the high velocity and acceleration constraints, there is no

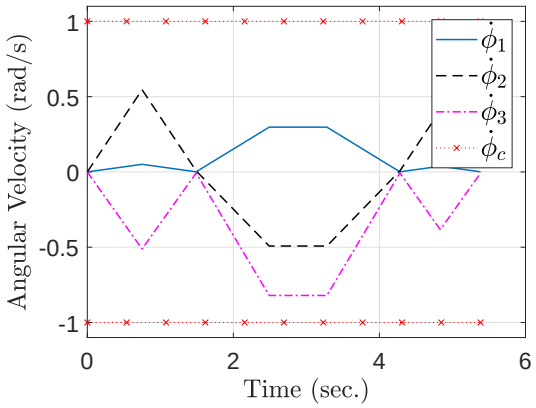

Figure 13. a)

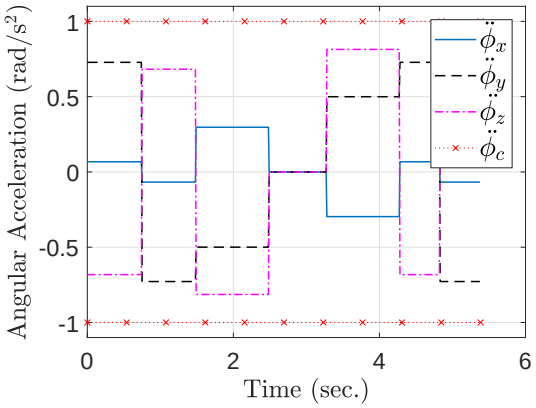

Figure 14. b)

Figure 15. Time histories of gyrostat a) angular velocity and b) angular acceleration when $|\alpha| > 0$.

coasting period for the ϕ_1 and ϕ_3 portions of the slew. However, there is a period of zero angular acceleration constant angular velocity for ϕ_2, which is reflected in Fig. 15. The time histories of quaternion and body-torque are shown in Fig. 18.

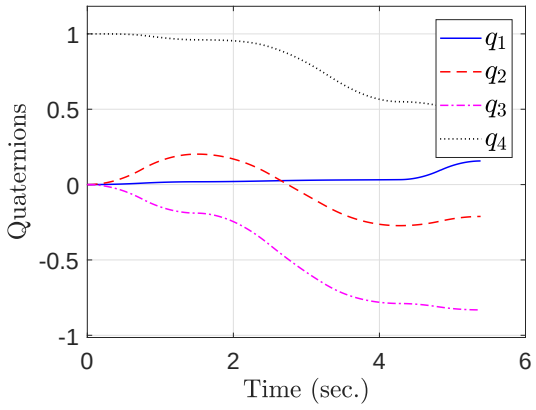

Figure 16. a)

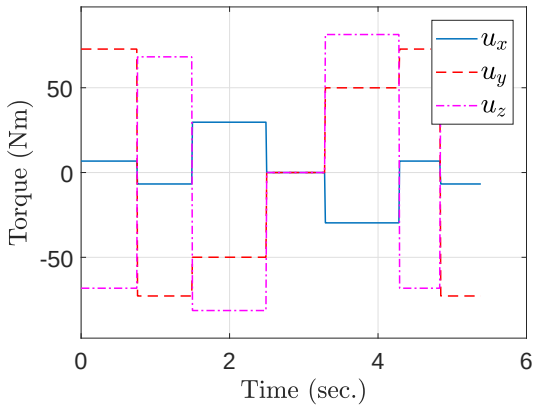

Figure 17. b)

Figure 18. Time histories of a) gyrostat-frame quaternions and b) body torques when $|\alpha| > 0$.

In case II, when $\alpha = 0$, we choose much more realistic constraints: 0.01 rad/s for angular velocity and 0.01 rad/s^2 for angular acceleration. The computed slew angles in this case are $(41.82, 180, 62.45)°$. The trajectory of the instrument boresight, is shown in Fig. 19. With

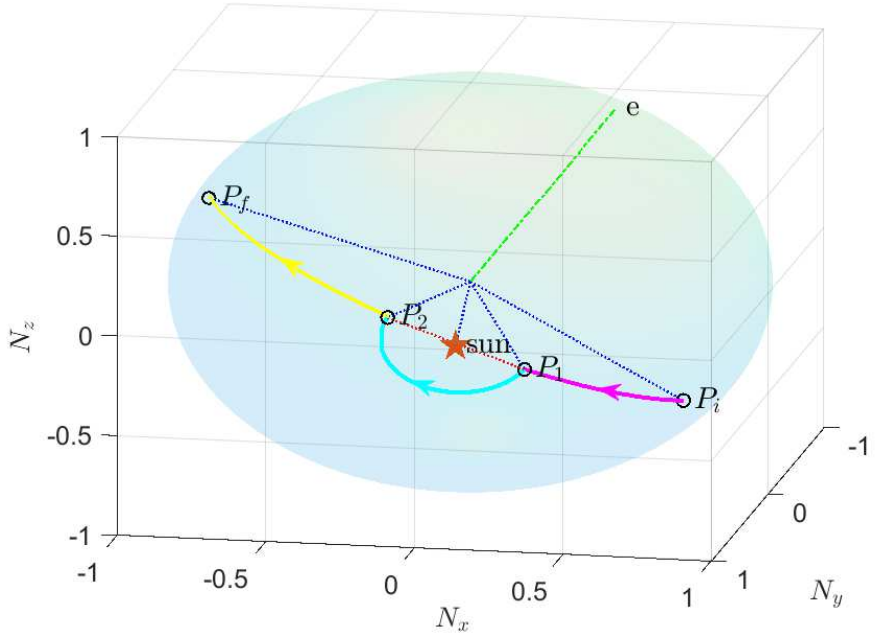

Figure 19. Trajectory of the instrument boresight during the entire slew when $\alpha = 0$.

smaller constraints, the simulation takes much longer to complete the slew maneuvers.

Figs. 22 and 25 show that the torque and acceleration applied are very short compared to the duration of the entire maneuver for case I ($|\alpha| > 0$), in contrast to Figs. 15 and 18 for case II ($\alpha = 0$). The spacecraft spends the majority of the time coasting at constant angular velocity, as seen in Fig. 22. Though the initial and final points are further apart in the gyrostat unit sphere to begin with, the simulation takes an order of magnitude longer to complete at almost 500 seconds for $\alpha = 0$, as opposed to about 5.5 seconds for $|\alpha| > 0$. The case shown here is much more realistic example that reflects real-world conditions. The results for both cases demonstrate that the angular velocity and acceleration never exceed the velocity and acceleration constraints for any axis.

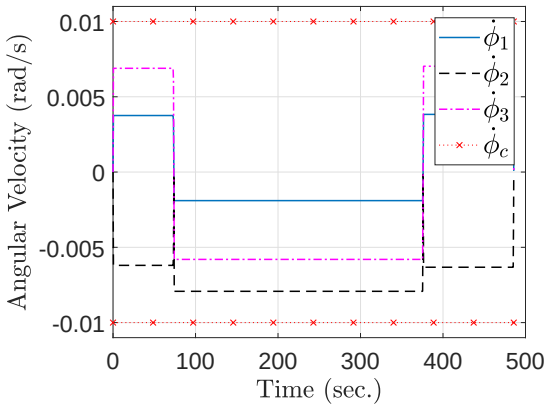

Figure 20. a)

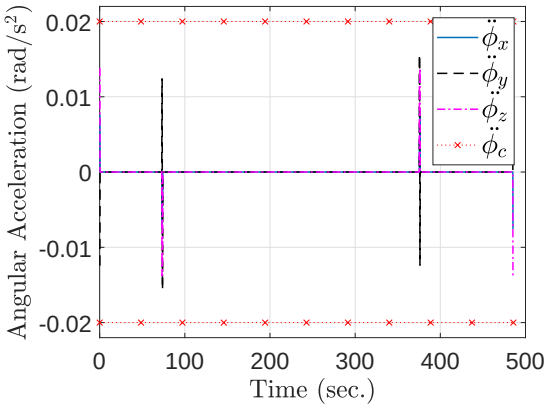

Figure 21. b)

Figure 22. Time histories of gyrostat a) angular velocity and b) angular acceleration when $\alpha = 0$.

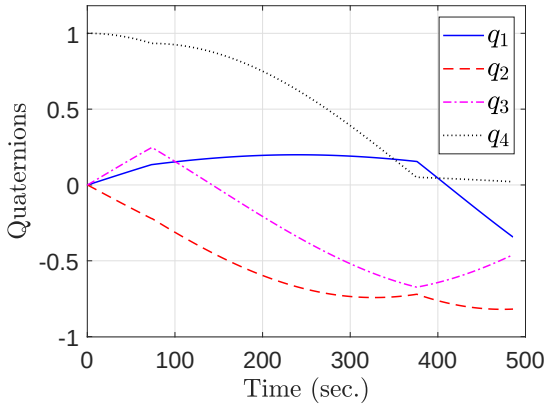

Figure 23. a)

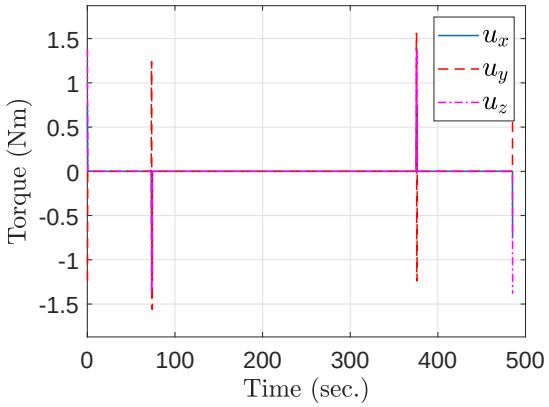

Figure 24. b)

Figure 25. Time histories of a) gyrostat-frame quaternions and b) body torques when $\alpha = 0$.

CONCLUSION

A new geometric approach for large-angle slew planning with pointing and actuator constraints is presented. The spacecraft has a single light-sensitive payload with control-torque and reaction wheels' angular momentum constraints. Furthermore, we assume that the initial and final attitudes, instrument line-of-sight vector, and sun vector are known. Then the desired or target-frame quaternions, angular velocities, and angular accelerations are derived based on the PMP. The proposed algorithm is intuitive, deterministic, and easy to implement. The main drawback of the proposed algorithm is its limitation for a single sensitive-payload. The feasibility of the proposed algorithm is demonstrated for two arbitrary cases and it has been investigated via extensive numerical simulations.

ACKNOWLEDGMENT

This research is supported by Maxar Space Infrastructure (Formerly Space Systems/Loral). The second author would like to acknowledge Luke DeGalan for his useful comments.

NOTATION

$\mathcal{G}$-frame	gyrostat body-fixed frame
${}^{\mathcal{N}}H^{\mathcal{G}/\mathcal{G}*}$	the total angular momentum of the gyrostat with respect to its center of mass
$I^{\mathcal{G}/\mathcal{G}^*}$	the mass-moment-of-inertia of the gyrostat
$I^{w/w*}$	the mass-moment-of-inertia of reaction wheels with respect to their center of masses
M_{max}	the maximum available torque along the eigenaxis
$\mathcal{N}$-frame	the Newtonian frame
${}_{\mathcal{N}}\hat{e}$	unit vector along the eigenaxis expressed in the $\mathcal{N}$-frame
${}_{\mathcal{G}}\hat{P}$	unit vector along the boresight of payload expressed in the $\mathcal{G}$-frame
${}_{\mathcal{N}}\hat{P}_i$	unit vector of the initial point expressed in the $\mathcal{N}$-frame
${}_{\mathcal{N}}\hat{P}_f$	unit vector of the final point expressed in the $\mathcal{N}$-frame
${}^{\mathcal{N}}q^{\mathcal{T}}$	quaternion of the $\mathcal{T}$-frame in the $\mathcal{N}$-frame
${}_{\mathcal{N}}\hat{S}$	unit vector of the sun vector in the $\mathcal{N}$-frame
$\mathcal{T}$-frame	the target frame
ϵ_p	Payload half-cone angle
${}^{\mathcal{N}}\alpha^{\mathcal{T}}$	angular acceleration of the $\mathcal{T}$-frame in the $\mathcal{N}$-frame
${}^{\mathcal{N}}\omega^{\mathcal{T}}$	angular velocity of the $\mathcal{T}$-frame in the $\mathcal{N}$-frame

REFERENCES

[1] C. R. McInnes, "Large angle slew maneuvers with autonomous sun vector avoidance," *Journal of Guidance Control Dynamics*, Vol. 17, 06 1994, pp. 875–877, 10.2514/3.21283.

[2] K. Spindler, "New Methods in On-Board Attitude Control (AAS 98-308)," Vol. 100, 01 1998.

[3] H. B. Hablani, "Attitude commands avoiding bright objects and maintaining communication with ground station," *Advances in the Astronautical Sciences*, 1998, 10.2514/2.4469.

[4] J. D. Biggs and L. Colley, "Geometric Attitude Motion Planning for Spacecraft with Pointing and Actuator Constraints," *Journal of Guidance, Control, and Dynamics*, 2016, 10.2514/1.G001514.

[5] E. Frazzoli, M. A. Dahleh, E. Feron, R. P. Kornfeld, and R. P. Kornfeld, "A Randomized Attitude Slew Planning Algorithm for Autonomous Spacecraft," *In AIAA Guidance, Navigation, and Control Conference*, 2001.

[6] D. Spiller, L. Ansalone, and F. Curti, "Particle Swarm Optimization for Time-Optimal Spacecraft Reorientation with Keep-Out Cones," *Journal of Guidance, Control, and Dynamics*, 2016, 10.2514/1.G001228.

[7] Y. Kim and M. Mesbahi, "Quadratically constrained attitude control via semidefinite programming," *IEEE Transactions on Automatic Control*, 2004, 10.1109/TAC.2004.825959.

[8] Y. Kim, M. Mesbahi, G. Singh, and F. Y. Hadaegh, "On the convex parameterization of constrained spacecraft reorientation," *IEEE Transactions on Aerospace and Electronic Systems*, 2010, 10.1109/TAES.2010.5545176.

[9] C. Sun and R. Dai, "Spacecraft Attitude Control under Constrained Zones via Quadratically Constrained Quadratic Programming," 2015, 10.2514/6.2015-2010.

[10] U. Lee and M. Mesbahi, "Quaternion based optimal spacecraft reorientation under complex attitude constrained zones," *Advances in the Astronautical Sciences*, 2014.

[11] M. Diaz Ramos and H. Schaub, "Kinematic Steering Law for Conically Constrained Torque-Limited Spacecraft Attitude Control," *Journal of Guidance, Control, and Dynamics*, Vol. 41, jul 2018, pp. 1990–2001, 10.2514/1.G002873.